Influence of Pore Formation and Its Role on the Tensile Properties of 17-4 PH Stainless Steel Fabricated by Laser Powder Bed Fusion

Dyuti Sarker, Usman Ali, Farid Ahmed, Reza Esmaeilizadeh, Ali Keshavarzkermani, Ehsan Marzbanrad, and Ehsan Toyserkani

Abstract Additive manufacturing (AM) is a promising technique due to the scope of producing complex objects from a digital model, where materials are deposited in the successive layers as distinct from the conventional manufacturing approaches. In this study, laser powder bed fusion (LPBF), a class of additive manufacturing (AM), is used to make testing samples with gas atomized 17-4 PH stainless steel (SS) powder at different process parameters in argon (Ar) environment. A thorough study on powder characteristics, such as particle size distribution, powder morphology, phase formation at different atmospheres, as well as the microstructure and tensile properties of the printed parts at various energy densities were carried out. The microstructural analysis discovered the presence of columnar dendrites with complete martensite phases regardless of the process parameters. A detailed X-ray computed tomography (CT) scan analysis on printed samples explored the correlation between the pores and energy density. The sample printed with adequate energy density obtained lower porosity (volume of pores: 2×10^4 to 9×104 μm^3, compared to 2×10^4 to 130×10^4 μm^3) resulting in maximum tensile strength and elongation of 770 MPa and 38%, respectively. Therefore, it is obvious that the quantity, size and shape of pores in the printed parts significantly affect the fracture mode.

Keywords 17-4 PH stainless steel · Laser powder bed fusion · Additive manufacturing · Martensite · Energy density

Introduction

Laser powder bed fusion (LPBF) also known as selective laser melting (SLM) is an AM technique where powder particles are selectively melted or fused with a point heat source to build parts using a layer by layer fabrication approach [1, 2]. Regardless

D. Sarker (✉) · U. Ali · F. Ahmed · R. Esmaeilizadeh · A. Keshavarzkermani · E. Marzbanrad · E. Toyserkani
Multi-Scale Additive Manufacturing Lab, Department of Mechanical and Mechatronics Engineering, University of Waterloo, 200 University Ave W, Waterloo, ON N2L 3G1, Canada
e-mail: dsarker@ryerson.ca

TMS 2021 150th Annual Meeting & Exhibition Supplemental Proceedings,
The Minerals, Metals & Materials Series,
https://doi.org/10.1007/978-3-030-65261-6_12

of the advantages of LPBF in the production of complex shapes [3], there still remain difficulties that restrict its extensive implementation in commercial applications. For example, there exists a lack of knowledge on the process–property correlation that assists the manufacturer to envisage the mechanical performance of the fabricated parts with adequate assurance. The inadequate understanding is ascribed by the rapid solidification which significantly influences the microstructure development and phase formation. The metallurgy in AM is manipulated by the characteristics of powder particles (powder composition, size distribution and morphology) as well as the cyclic thermal loading during the process. Other factors that affect the structural development are laser power, laser beam shape/intensity, laser scan pattern, chamber atmosphere as well as machine features [4–8] which govern the solidification kinetics. For the entire process, the heating and cooling rates dominate further precipitation kinetics, phase transformation and grain growth [9]. Mechanical properties of LPBF processed parts are stimulated by their microstructure and crystallographic phases, which are actually influenced by thermal characteristics such as cooling/solidification rates and thermal gradients [10].

Several researchers have worked on the microstructure, phase transformation, porosity level, and mechanical property of LPBF processed 17-4 PH SS. Among them, Pasebani et al. [11] studied the effects of powder atomizing media (water atomization vs. gas atomization) on phase transformation and mechanical properties of laser melted 17-4 PH SS parts. Gas atomized powder formed martensitic phases, whereas water atomized powder revealed dual phases of martensite and austenite. The microstructural study by Cheruvathur et al. [12] reported the dendritic structure with martensite and 50% retained austenite, where niobium carbide is aligned along the interdendritic boundaries. More microstructural study of LPBF processed 17-4 PH SS have been presented by Sun et al. [7, 13] and LeBrun et al. [14]. In a study by Facchini et al. [15], the microstructure development of 17-4 PH SS in the LPBF technique was presented, where the gas atomization and printing atmospheres were Ar. From their work, mostly austenitic phases were reported which transformed into martensite during tensile deformation. On the other hand, Murr et al. [16] have investigated the Ar and N_2 atmospheric effect in the LPBF technique on the martensite and austenite phase formation, respectively. The presence of both martensite and retained austenite in the LPBF processed parts in the N_2 build atmosphere implies that N_2 can influence the stability of the austenite. Rafi et al. [17] also worked on the mechanical and microstructural development of 17-4 PH SS, in the LPBF technique using both Ar and N_2 atmosphere. Their results focused on the formation of martensite and austenite phases, which are influenced by powder chemistry, fabrication atmosphere and grain morphology. However, Starr et al. [18] showed austenite phases and their transformation to martensite during LPBF of 17-4 PH SS powders. From their work, it is emphasized that, based on the powder chemistry, LPBF process parameters, post-process conditions, the resulted microstructure and the phase compositions could be much different than those manufactured using conventional techniques.

Therefore, the laser input energy density can also affect the build part microstructure. The presence of porosity in the microstructure experienced due to the different energy densities. With appropriate energy input, pores and un-melted conditions can

be alleviated to some extent in LPBF. Our recent study on 17-4PH SS shows that initial state of the powder is controlling the mechanical properties of the printed parts [19]. However, to the authors' best knowledge, there was no comprehensive study on the correction between energy density and tensile property of the 17-4 PH SS. It is also not clear how the energy density influences the morphologies like size and shape of the porosity which affects the mechanical properties of the printed parts. In this work, the effect of energy densities on LPBF processed 17-4 PH SS is explored based on the details of microstructural features such as phases, defects specifically the porosity, etc. and made a correlation with mechanical properties leading to the fracture mechanisms.

Materials and Experiments

The sample fabrication was carried using EOS M290 (EOS GmbH, Krailling, Germany), LPBF system and 17-4 PH SS powder. The ranges of particle size of the powder were between 16 μm and 63 μm. Samples were printed using recycled powder in an Ar atmosphere with a layer thickness of 40 μm, hatch spacing 90 μm. Details of the printing strategy with build plate dimension are presented in previous works [19, 20]. The specimens in all prints were built using different laser powers, scanning speeds and with a constant hatch distance. Among the all printed conditions, three samples at different input parameters are considered for detail study, i.e. sample I (170 W, 1000 mm/s: 47 J/mm^3), sample II (170 W, 800 mm/s: 59 J/mm^3), sample III (195 W, 800 mm/s: 68 J/mm^3). To explore the effect of process parameters on mechanical property, tensile samples were built using three different energy densities.

Powder and printed samples microstructure were examined using scanning electron microscope (SEM) and electron backscatter diffraction (EBSD). The printed samples were prepared following standard metallographic techniques and etching with a mixture of 2.5 ml ethanol, 2.5 g picric acid, and 5 ml hydrochloric acid. EBSD was conducted using JEOL7000F SEM, with operational Oxford EBSD detector. The tensile tests were conducted at a crosshead speed of 0.45 mm/min in accordance with ASTM E8 standard, using Instron 8872 equipped with a 25 KN load cell. To obtain the distribution of the porosity, X-ray computed tomography (CT) was performed using scan (Zeiss Xradia 520 Versa, Oberkochen, Germany). For an applied voltage of 140 kV, 801 2D slices of specimens were subjected to 10 W X-ray radiation for 1 s.

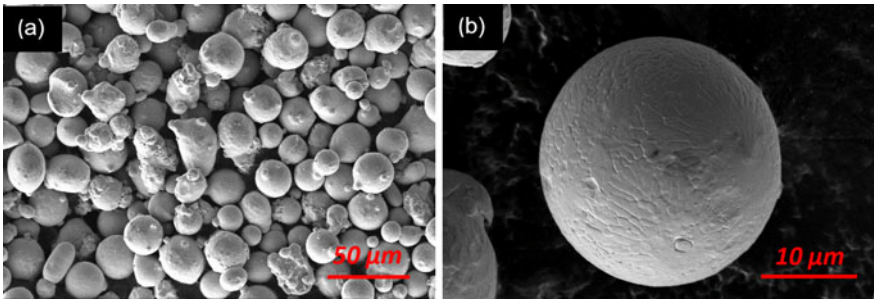

Fig. 1 SEM micrograph shows powder morphology of used powders: **a** multiple particles at low magnification, **b** surface morphology of the single particle at high magnification. (Color figure online)

Results

Powder Morphology

Powders, as feedstock materials, must be carefully chosen in terms of quality and cost in connection with the AM process used in the part fabrication. The powder morphology, both agglomerated and the cross-section of the powders, was studied using SEM, as presented in Fig. 1. From the micrograph, most of the particles of powders are spherical in shape, as shown in Fig. 1a. The magnified single spherical particle in Fig. 1b exhibits various orientation of dendritic structure on its outer surface.

Microstructure

The SEM micrograph shows similar structural features in LPBF processed 17-4 PH SS in three different samples, where samples I, II, and III show typical columnar grains, as obvious in Figs. 2a–c, respectively. The columnar grains are formed in the solidified parts and their cross-sections along the building direction shows martensitic laths inside the grains. The martensitic laths are clearly visible in magnified image of sample III, presented in Fig. 2d. The solidified parts are characterized by columnar grains oriented in various directions. The martensitic laths of various orientations are also seen within the grains. The structural feature implies that the direction of dendritic progression is parallel to the heat flow and develops a higher orientation tendency in the solidified parts [17]. On the martensitic laths, in Fig. 2d, white sparking precipitates are visible. This type of precipitates was also reported by Wang et al. [21], in LPBF processed 17-4 PH SS.

The IPF orientation of the printed sample I obtained using EBSD is shown in Fig. 3. The EBSD images fall within the longitudinal cutting plane, where columnar

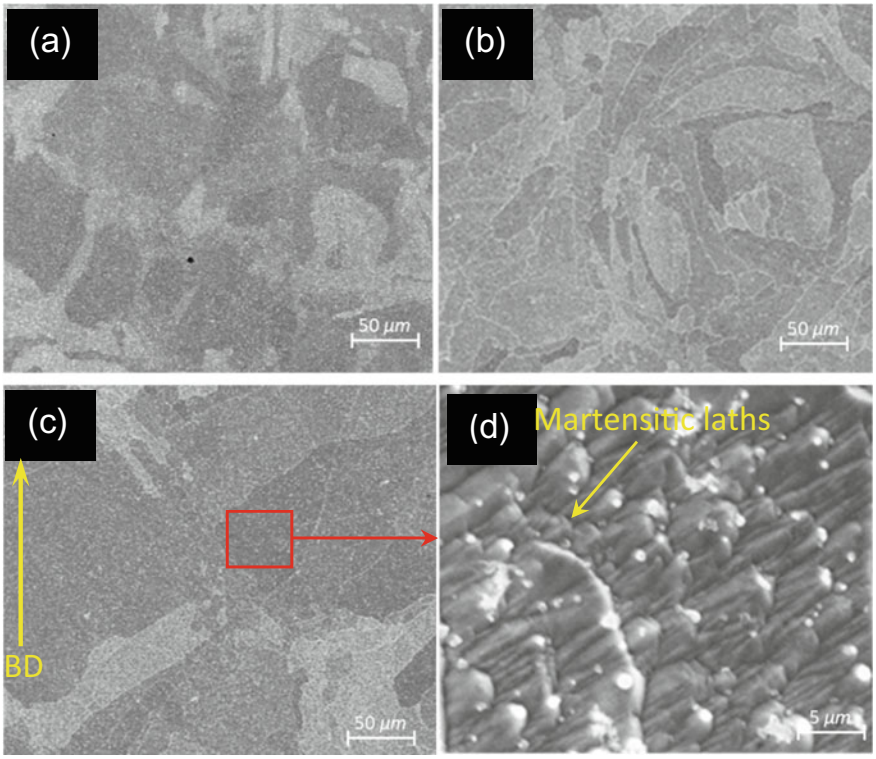

Fig. 2 SEM micrograph showing similar structural features in 17-4 PH printed parts at different parameters, **a** sample I, **b** sample II, **c** sample III, and **d** magnified view of sample III (along the building direction (BD)). (Color figure online)

grains are perpendicular (Fig. 3a) and parallel (Fig. 3b) to the build direction. This emphasizes that columnar grains form in multiple direction and grow parallel to the heat flow. The columnar grains along the build directions appears like globular shapes, whereas, from normal direction, elongated shapes are evident. The inverse pole figures presented in the bottom of the images (Fig. 3a and b) are identical and confirm the presence of random texture in the solidified parts.

The EBSD image mapping in Fig. 3c (along the build direction like 3a) is showing the distribution of low-angle grain boundaries (LAGB) and high-angle grain boundaries (HAGB), which correspond to red and black colors, respectively. The intersecting angle between grains below 15 ° is considered as LAGB, whereas greater than 15 ° is the HAGB. The grain boundary mapping shows about 65% percentage of HAGB, while only 35% grain boundaries are LAGB that indicates the remelting layers during printing. Similar type results were reported by Wang et al. [21].

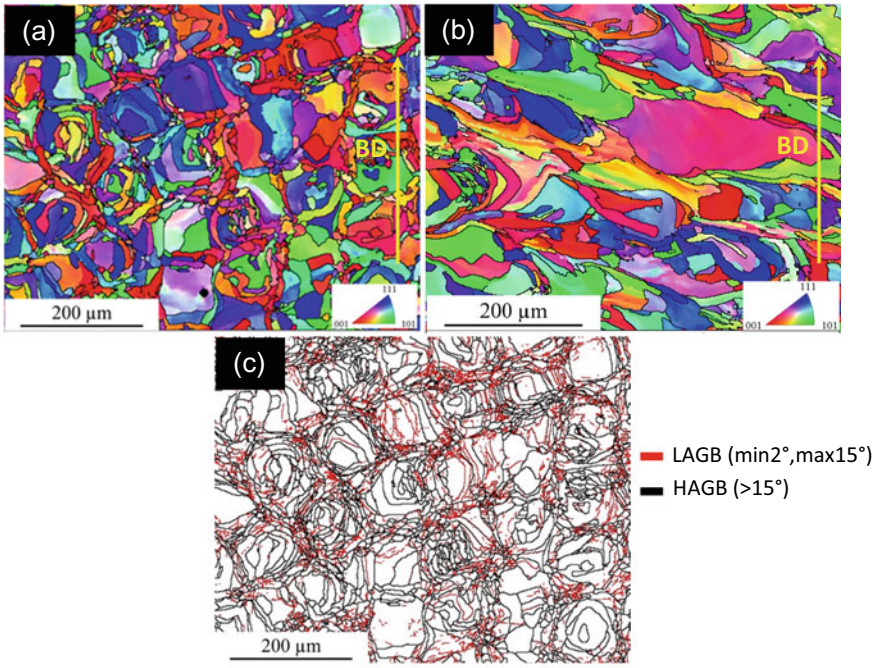

Fig. 3 EBSD image mapping of LPB processed 17-4 PH steel, **a** along the build direction, **b** normal to the build, **c** image mapping showing LAGB and HAGB. (Color figure online)

Porosity Distribution

CT scan results of Samples I, II, and III are presented in Fig. 4. The three samples printed in different energy densities show significant variations in pore distribution.

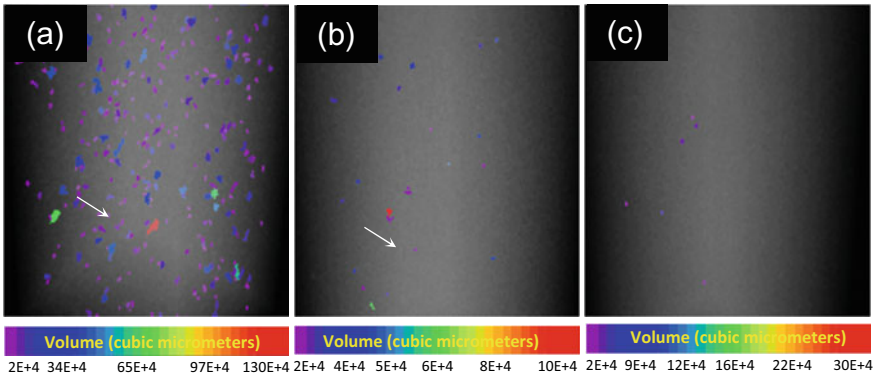

Fig. 4 Porosity distribution in LPBF processed samples at various energy density, **a** Sample I, **b** Sample II, and (III), **c** Sample III. (Color figure online)

The variation of the volumes of pores detected in the printed samples is presented in the legends. The scale bar corresponds to each color indicates pore volume in cubic micrometer. It is evident that the quantity and quality of the pores are linked with the energy density of the input parameters. At lower energy density, Sample I (47 J/mm) shows higher porosity than the Sample II (59 J/mm) and III (67 J/mm), respectively. In Sample I, the elongated and irregular pores are greater in number, as well as with larger volume sizes, which ranges from 2×10^4 to 130×10^4 μm^3. Sample II possesses smaller quantity of pores, and volume size ranges from 2×10^4 to 10×10^4 μm^3. In Sample III, very few quantities of spherical pores are observed, and from the scale bar, it is evident that volume size of these pores ranges from 2×10^4 to 9×10^4 μm^3.

Tensile Property

Figure 5 shows the tensile properties includes yield strength (YS), ultimate tensile strength (UTS), and elongation (El) for different energy density. The three different energy densities exhibited significant changes in the tensile properties. In general, sample (Sample I) fabricated with lower energy density (47 J/mm) exhibit poor tensile property. In contrast, Samples II and III with increasing energy density (59 and 68 J/mm, respectively) show greater tensile properties. The ultimate tensile strength (UTS) is lower in Sample I (665 MPa), compared to Sample II (701 MPa) and Sample III (773 MPa). The ductility also improves from Sample I (23%) to Sample II (38%) and Sample III (35%). A small increase in elongation is observed in Sample II than Sample III, exhibiting better ductility with minor amount of pore formation. In Sample III, higher YS (753 MPa) is observed than Sample II (688 MPa) and Sample I (646 MPa).

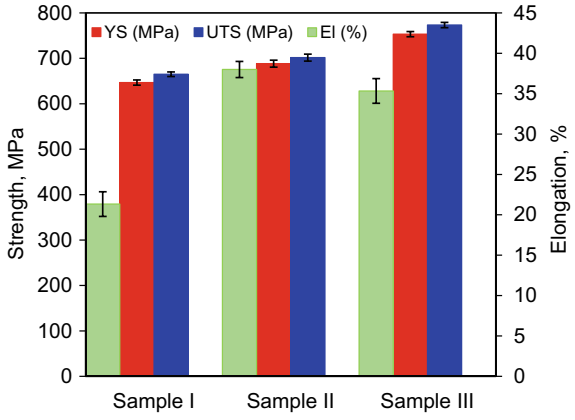

Fig. 5 Engineering stress–strain curves, values of yield strength (YS), ultimate tensile strength (UTS), and elongation (El) of LPBF processed 17-4 PH SS, at three different energy densities. (Color figure online)

Discussion

In current study, the phase formed in the LPBF processed 17-4 PH SS shows only martensitic structure for both powder and the printed samples. Moreover, it is reported that the LPBF processed 17-4 PH SS samples possess austenitic phase, depending on the process environment [11, 16, 17, 21, 22]. The presence of both martensite and retained austenite can be explained by the experimental atmosphere during powder atomization followed by LPBF of 17-4 PH SS. However, the samples in the present study were printed in Ar atmosphere. So, identical microstructural features are obvious at different energy densities (Fig. 2). The structure of elongated columnar grains and martensitic lath formation is due to the heat dissipation along the build direction. Similar columnar grains are presented in the LPBF processed 17-4 PH SS samples, where the result indicates that dendritic growth approaches parallel to the heat flow showing higher orientation tendency in the melt zone [17]. Moreover, the EBSD results emphasize the grain morphology and the orientation of the grains together with the grain boundary angles. The crystallographic orientation of columnar dendrites was color coded in the EBSD map (Fig. 3a and b), where different color corresponds to different orientations. In directional solidification, the primary dendrites propagate in the opposing direction of the thermal gradient, which also perpendicular to the mushy zone are categorized by various growth directions.

Porosity is one of the common defects in AM parts, which can adversely affect the mechanical properties. The source of the porosities could be various, i.e., powder made, process made or a product of solidification [23]. Generally, the spherical pores are generated from the entrapped gas because of the vapor pressure of the entrapped gas, stimulated by manufacturing process of both powder and the printed parts [24]. The irregular shaped pores are the result of some factors, such as cracks caused by thermal stress, partial melting of powders, balling phenomena, which occurs when melt pools are unable to defeat surface tension and results partial coverage for the following layers [25]. Because of the irregularity in the shape, these pores are bigger in size compared to the spherical pores [26]. The elongated pores are generated from the inadequate melting of powder within layer into layer initiating cracking and elongated voids [27]. Therefore, the presence of irregular and elongated pores in Sample I are associated with the inadequate energy density through the LPBF process, leading to incomplete melting of powders. Process made porosity can impact other factors, such as powder consolidation, which may influence to an inaccurately packed powder bed to completely dense parts [28]. The distributed powder on the powder bed may contain particles bigger in diameter than the layer thickness and through melting consolidated into a layer of proper height. The samples printed in different energy densities show a significant change in tensile properties. The better tensile strength and ductility can be attributed with the size and shape of the pores formed in the printed samples. The bigger size of irregular and elongated pores in Sample I caused premature failure results poor tensile property. In contrast, the smaller size of irregular pores in Sample II promotes a combination of brittle and ductile failure.

The negligible smallest size of pores in Sample III can resolve much load during tensile testing and resulting ductile failure with better tensile property.

Conclusions

This study explains how the energy density influences the size and shape of the porosity which affects the tensile properties of the printed parts. Samples of 17-4 PH SS were printed using LPBF in Ar atmosphere at three different energy densities using recycled gas atomized powders. Through the experimental results, microstructure and tensile properties are affected by energy densities. From the above discussion, it can be summarized as follows:

(a) Unlike other research works, the samples printed in Ar atmosphere shown complete martensitic transformation. The columnar dendrites and martensite phases are observed in all three printed samples (Samples I, II, and III).
(b) The sample printed with lower energy density (47 J/mm^3) formed greater number of pores with larger volume sizes. With higher energy density (59 J/mm^3 and 67 J/mm^3), the pore content reduces as well as the volume of the individual pores.
(c) As the Sample I, exhibits significant volume of pores, they did not pass through the necking, which indicates premature failure. On the other hand, the lower pore density in Samples II and III show necking with higher tensile property. Therefore, both the pore quantity and shapes influence the tensile property, which is evident in Sample III through higher tensile strength of 770 MPa and elongation of 38%.

Acknowledgements This work was supported by funding from the Natural Sciences and Engineering Research Council of Canada (NSERC), the Federal Economic Development Agency for Southern Ontario (FedDev Ontario) and Siemens Canada Limited. The authors would like to acknowledge the support from Jerry Ratthapakdee and Karl Rautenberg for helping with design and printing of LPBF parts. In addition, the authors would like to acknowledge the encouragement and support from the members of Multi-Scale Additive Manufacturing group (MSAM), Fatigue and Stress Analysis Lab (FATSLAB) at the University of Waterloo and Canadian Center of Electron Microscopy members (CCEM).

References

1. Gibson I, Rosen DW, Stucker B (2010) Additive manufacturing technologies: rapid prototyping to direct digital manufacturing
2. Kruth JP, Levy G, Klocke F, Childs THC (2007) Consolidation phenomena in laser and powder-bed based layered manufacturing. CIRP Ann Manuf Technol. https://doi.org/10.1016/j.cirp.2007.10.004

3. Waller JM, Parker BH, Hodges KL, Burke ER, Walker JL (2014) Nondestructive evaluation of additive manufacturing state-of-the-discipline report, NASA/TM-2014-218560, https://doi.org/10.13140/rg.2.1.1227.9844
4. Cherry JA, Davies HM, Mehmood S, Lavery NP, Brown SGR, Sienz J (2015) Investigation into the effect of process parameters on microstructural and physical properties of 316L stainless steel parts by selective laser melting. Int J Adv Manuf Technol 76(5–8):869–879. https://doi.org/10.1007/s00170-014-6297-2
5. Yusuf SM, Gao N (2017) Influence of energy density on metallurgy and properties in metal additive manufacturing Influence of energy density on metallurgy and properties in metal additive manufacturing. Mater Sci Technol 33(11):1269–1289. https://doi.org/10.1080/02670836.2017.1289444org/10.1080/02670836.2017.1289444
6. Rashid R, Masood SH, Ruan D, Palanisamy S, Rahman Rashid RA, Brandt M (2017) Effect of scan strategy on density and metallurgical properties of 17-4PH parts printed by selective laser melting (SLM), J Mater Process Technol 249:502–511, https://doi.org/10.1016/j.jmatprotec.2017.06.023
7. Sun Y, Hebert RJ, Aindow M (2018) Effect of heat treatments on microstructural evolution of additively manufactured and wrought 17-4PH stainless steel. Mater Des 156:429–440. https://doi.org/10.1016/j.matdes.2018.07.015
8. Keshavarzkermani A et al (2019) An investigation into the effect of process parameters on melt pool geometry, cell spacing, and grain refinement during laser powder bed fusion, Opt Laser Technol, https://doi.org/10.1016/j.optlastec.2019.03.012
9. Cantor B, Kim WT, Bewlay BP, Gillen AG (1991) Microstructure - cooling rate correlations in melt-spun alloys. J Mater Sci 26(5):1266–1276. https://doi.org/10.1007/BF00544465
10. Selcuk C (2011) Laser metal deposition for powder metallurgy parts, Powder Metall, https://doi.org/10.1179/174329011x12977874589924
11. Pasebani S, Ghayoor M, Badwe S, Irrinki H, Atre SV (2018) Effects of atomizing media and post processing on mechanical properties of 17-4 PH stainless steel manufactured via selective laser melting, Addit Manuf, https://doi.org/10.1016/j.addma.2018.05.011
12. Cheruvathur S, Lass EA, Campbell CE (2016) Additive manufacturing of 17-4 PH stainless steel: post-processing heat treatment to achieve uniform reproducible microstructure, JOM, https://doi.org/10.1007/s11837-015-1754-4
13. Sun Y, Hebert RJ, Aindow M (2018) Non-metallic inclusions in 17-4 PH stainless steel parts produced by selective laser melting, Mater Des, https://doi.org/10.1016/j.matdes.2017.11.063
14. LeBrun T, Nakamoto T, Horikawa K, Kobayashi H (2015) Effect of retained austenite on subsequent thermal processing and resultant mechanical properties of selective laser melted 17-4 PH stainless steel. Mater Des 81:44–53. https://doi.org/10.1016/j.matdes.2015.05.026
15. Facchini L, Vicente N, Lonardelli I, Magalini E, Robotti P, Alberto M (2010) Metastable austenite in 17-4 precipitation-hardening stainless steel produced by selective laser melting. Adv Eng Mater 12(3):184–188. https://doi.org/10.1002/adem.200900259
16. Murr LE et al (2012) Microstructures and properties of 17-4 PH stainless steel fabricated by selective laser melting. J Mater Res Technol 1(3):167–177. https://doi.org/10.1016/S2238-7854(12)70029-7
17. Rafi HK, Pal D, Patil N, Starr TL, Stucker BE (2014) Microstructure and mechanical behavior of 17-4 precipitation hardenable steel processed by selective laser melting, J Mater Eng Perform, https://doi.org/10.1007/s11665-014-1226-y
18. Starr TL, Rafi K, Stucker B, Scherzer CM (2012) Controlling phase composition in selective laser melted stainless steels
19. Ali U et al (2019) Identification and characterization of spatter particles and their effect on surface roughness, density and mechanical response of 17-4 PH stainless steel laser powder-bed fusion parts, Mater Sci Eng A, https://doi.org/10.1016/j.msea.2019.04.026
20. Ahmed F, Ali U, Sarker D, Marzbanrad E, Choi K, Mahmoodkhani Y (2019) Study of powder recycling and its e ff ect on printed parts during laser powder-bed fusion of 17-4 PH stainless steel, J Mater Process Tech, November, p 116522, https://doi.org/10.1016/j.jmatprotec.2019.116522

21. Wang D et al (2019) The effects of fabrication atmosphere condition on the microstructural and mechanical properties of laser direct manufactured stainless steel 17-4 PH. J Mater Sci Technol. https://doi.org/10.1016/j.jmst.2019.03.009
22. Gu H, Gong H, Pal D, Rafi K, Starr T, Stucker B (2013) Influences of energy density on porosity and microstructure of selective laser melted 17– 4PH stainless steel, https://doi.org/10.1007/s13398-014-0173-7.2
23. Kruth JP, Wang X, Laoui T, Froyen L (2003) Lasers and materials in selective laser sintering, Assem Autom. https://doi.org/10.1108/01445150310698652
24. Zhao X, Chen J, Lin X, Huang W (2008) Study on microstructure and mechanical properties of laser rapid forming Inconel 718, Mater Sci Eng A, https://doi.org/10.1016/j.msea.2007.05.079
25. Gu DD, Meiners W, Wissenbach K, Poprawe R (2012) Laser additive manufacturing of metallic components: materials, processes and mechanisms. Int Mater Rev 57(3):133–164. https://doi.org/10.1179/1743280411Y.0000000014
26. Sames WJ, List FA, Pannala S, Dehoff RR, Babu SS (2016) The metallurgy and processing science of metal additive manufacturing. Int Mater Rev 61(5):315–360. https://doi.org/10.1080/09506608.2015.1116649
27. King WE et al (2014) Observation of keyhole-mode laser melting in laser powder-bed fusion additive manufacturing. J Mater Process Technol 214(12):2915–2925. https://doi.org/10.1016/j.jmatprotec.2014.06.005
28. Körner C, Bauereiß A, Attar E (2013) Fundamental consolidation mechanisms during selective beam melting of powders, Model Simul Mater Sci Eng, https://doi.org/10.1088/0965-0393/21/8/085011